Eur. Phys. J. A **25**, s01, 23–26 (2005)
DOI: 10.1140/epjad/i2005-06-189-6

EPJ A direct
electronic only

New mass measurements at the neutron drip-line

H. Savajols[1,a], B. Jurado[1], W. Mittig[1], D. Baiborodin[2], W. Catford[3], M. Chartier[4], C.E. Demonchy[1,4], Z. Dlouhy[2], A. Gillibert[5], L. Giot[1,6], A. Khouaja[1,10,12], A. Lépine-Szily[8] S. Lukyanov[9], J. Mrazek[2], N. Orr[6], Y. Penionzhkevich[9], S. Pita[1,11], M. Rousseau[1,7], P. Roussel-Chomaz[1], and A.C.C. Villari[1,13]

[1] GANIL, BP 55027, F-14075 Caen Cedex 5, France
[2] Nuclear Physics Institute ASCR, 25068, Rez, Czech Republic
[3] University of Surrey, Nuclear Physics Department, Guilford, GU27XH, UK
[4] University of Liverpool, Department of Physics, Liverpool, L69 7ZE, UK
[5] CEA/DSM/DAPNIA/SPHN, CEN Saclay, F-91191 Gif-sur Yvette, France
[6] LPC - ISMRA and University of Caen, F-6704 Caen, France
[7] IReS - Strasbourg, 23 rue du loess, BP 28, F-67037 Strasbourg, France
[8] University of São Paulo IFUSP, C.P. 66318, 05315-970 São Paulo, Brazil
[9] FLNR, JINR Dubna, P.O. Box 79, 101000 Moscow, Russia
[10] LNS-INFN, 44 S. Sofia, I-95129 Catania, Italy
[11] Collège de France, 11 Place Marcelin Berthelot, F-75231 Paris Cedex 05, France
[12] LPTN Faculty of Sciences, El Jadida BP 20, 24000 El Jadida, Morocco
[13] Physics Division, Argonne National Laboratory, 9700 S. Cass Av., Argonne, IL 60439, USA

Received: 5 May 2005 /
Published online: 11 August 2005 –

Abstract. A new SPEG mass measurement experiment has been performed to determine masses closer to the neutron drip-line in the mass region $A \sim 10$–50. The precision of 37 masses has been improved and 8 masses were measured for the first time. The region covered was motivated by the study of shell structure and of shape coexistence in the region of closed shells $N = 20$ and $N = 28$. The evolution of the two neutron separation energies and the shell correction energy have been studied as a function of the neutron number. The results thus obtained provide a means of identifying, in exotic nuclei, new nuclear structure effects that are well illustrated by the changes of the conventional magic structure.

PACS. 21.10.Gv Mass and neutron distributions – 21.10.Dr Binding energies and masses

1 Introduction

The extension of known experimental properties up to very neutron rich nuclei is of fundamental interest particularly for nuclear theory models which have been mainly derived based on properties observed close to stability. New experimental data deepens our understanding of nuclear structure evolution towards large fluid asymmetries. The structure of neutron-rich nuclei is today the focus of many theoretical and experimental efforts. Deformations, shape coexistence or variations in the spin-orbit strength emerging with the evolution of the neutron-to-proton ratio can provoke the existence of magic numbers different from those observed near stability. Such behaviour has also been proven to be important in other domains. As seen, for example, in nucleo-synthesis, where a quenching of shell effects, and consequently of spin orbit splitting, can provide for a better agreement between model calculations and observed abundances [1].

In this context, the measurement of masses (or binding energy) of nuclei far from stability is of fundamental interest for our understanding of nuclear structure. Their knowledge over a broad range of the nuclear chart is an excellent and severe test of nuclear models. This is why considerable experimental and theoretical efforts have been and are invested in this domain.

In this contribution, we present new mass measurements for neutron-rich nuclei in the region defined by ($5 < N < 28$; $7 < Z < 18$) obtained with the spectrometer SPEG at GANIL. These data correspond to the most exotic nuclei presently attainable in this region and provide first indications of new regions of deformation or shell closures very far from stability.

2 Experimental set-up

The method used is a direct time of flight combined with rigidity analysis technique (see fig. 1). The exotic nuclides are produced by bombarding a ^{181}Ta production target

[a] Conference presenter; e-mail: savajols@ganil.fr

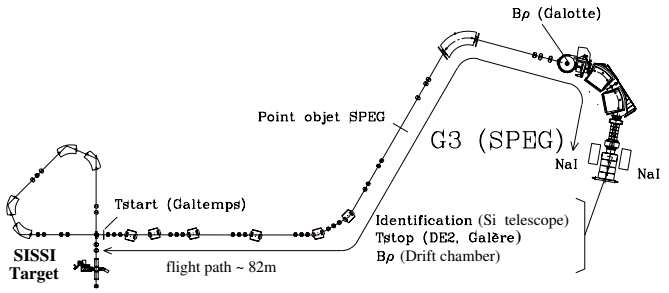

Fig. 1. Experimental set-up.

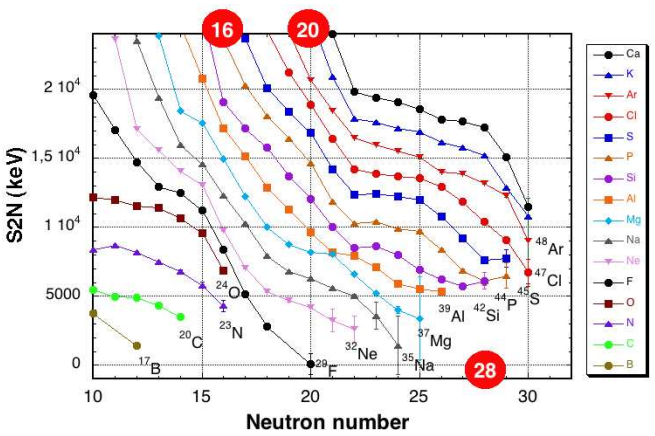

Fig. 2. Experimental S_{2n} values as a function of the neutron number N in the region of $N = 20$ and $N = 28$ shell closures .

with an intense ^{48}Ca primary beam (6×10^{11} pps) at intermediate energy, 60 $A \cdot$ MeV. The dominant mechanism at this energy is projectile fragmentation, after which the forward-directed fragments are selected in flight by the α-shaped spectrometer and transported to the high-resolution spectrometer SPEG [2]. The very broad elemental and isotopic distributions resulting from such reactions combined with the fast in-flight electromagnetic selection can provide the mapping of an entire region of the nuclear mass surface in a single measurement.

The ^{181}Ta production target, placed between the two superconducting solenoids (SISSI) of GANIL [3], rotated at 2000 rpm, was composed of three different sectors with thickness of 550 mg/cm^2 (89%), 450 mg/cm^2 (10%) and 250 mg/cm^2 (1%). This ensured a sufficient production of both very and less exotic nuclei, allowing to measure a broad range of reference masses from which unknown masses are derived. The mass is deduced from the relation

$$B\rho = \frac{\gamma m_0 v}{q},$$

where $B\rho$ is the magnetic rigidity of a particle of rest mass m_0, charge q and velocity v and γ the Lorentz factor. This technique requires only a precise determination of the magnetic rigidity and the velocity of the ion, which is determined from a time-of-flight measurement.

The time of flight (ToF) is measured using a pair of microchannel plate detector systems located near the production target (start signal) and at the final focal plane of SPEG (stop signal). The flight times are typically of the order of 1 μs for a path 82 m long. The intrinsic resolution of the start and stop detectors are of the order of 100–200 ps (FWHM) leading to a time-of-flight resolution of $\Delta t/t \sim 2 \cdot 10^{-4}$.

The magnetic rigidity, δ, of each ion is derived from two horizontal position measurements. The first measurement is performed by a thin position-sensitive microchannel plate system located at the dispersive image planes of the analysing magnet, i.e. at the conventional target chamber where the dispersion in momentum is large (10 cm/%). The second is made by two drift chambers used after the spectrometer. Thus reconstruction of the trajectories of each ion is possible and we accurately determine the value of the magnetic rigidity independantly of the object size. A momentum resolution of 10^{-4} is commonly achieved.

The identification of each ion arriving at the focal plane of SPEG is achieved by the measured ToF and the energy loss and total energy signals from a detector telescope.

As a check that deduced masses are not affected by the existence of isomers, the present mass measurement are combined with a detection of delayed γ rays by a 4π NaI array surrounding the telescope.

A mass resolution corresponding typically to $\pm$ 3 MeV of the mass excess can be obtained from the combination of the time-of-flight and the magnetic rigidity measurement. For a nucleus $A = 40$, the final uncertainties range from 100 keV for thousands of events (nuclei relatively close to stability) to 1 MeV for tens of events (nuclei approaching the ends of isotopic chains).

3 Results of mass measurements

From this experiment and its subsequent analysis, the masses of 80 neutron-rich nuclei have been measured. The precision of 37 masses has been significantly improved while 8 masses were measured for the first time. Details of the analysis technique can be found in already published papers [4,5].

The separation energy of the 2 last neutrons corresponding to a derivative of the mass surface, S_{2n}, derived from the current and previous measurements are displayed in fig. 2. A more direct way to see shell effects on nuclear masses is to subtract from the mass excesses the contribution of the macroscopic properties of the nuclei. Here we have used the finite range liquid drop model of [6]. The difference —the microscopic or Shell Correction Energy (SCE)— is plotted in fig. 3 for $Z = 14$ to $Z = 20$ isotopes and fig. 4 for $Z = 8$ to $Z = 13$ isotopes. As can be seen for both observables, i.e. experimental S_{2n} and SCE, the Ca isotopes ($Z = 20$) show the typical behavior of the filling of shells with the two shell closures at $N = 20$ and $N = 28$; sharp decrease of the S_{2n} at $N = 20$ and a slow decrease of S_{2n} as the $1f_{7/2}$ shell is filled and SCE minima at $N = 20$ and $N = 28$. In the rest of the article, the standard behavior represented by the Ca chain will be taken as reference.

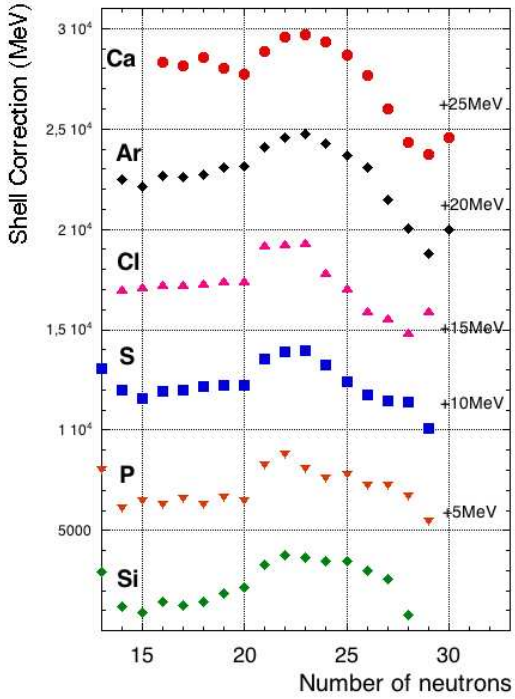

Fig. 3. Shell corrections as defined in the text of the mass of Si, P, S, Cl, Ar and Ca isotopes.

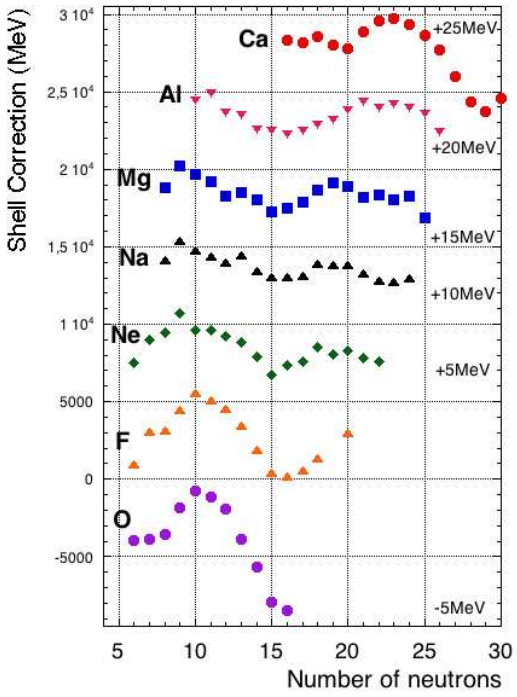

Fig. 4. Shell corrections as defined in the text of the mass of O, F, Ne, Na, Mg, Al and Ca isotopes.

3.1 The N = 28 region

Contrary to the Ar and K isotopes, both S_{2n} and SCE values of the Cl, S, P and Si isotopic chains differ around $N = 28$ from the standard behavior represented by the Ca chain. A discontinuity in the S_{2n} slope when filling the $\nu 1f_{7/2}$ shell (from $N = 20$ to $N = 28$) is strongly pronounced for the Cl, S and P isotopes. This trend is attenuated for the Si and Al chains. This overbinding, already observed in our previous mass measurement experiment [7], but with large uncertainties, was attributed to deformed ground state configurations. The observation, in the same experiment, of a low excited isomeric state in ^{43}S [7], confirmed the analysis of the masses and constituted the first shape coexistence in that region. More detailed informations have been obtained for these nuclei by other experimental probes, *i.e.* Coulomb excitation measurement for the S isotopes [8,9] and in beam gamma spectroscopy experiment [10]; both conclude for deformed ground state configurations.

Beyond $N = 28$, the isotopic P and S isotopic chains show a clear increase of the S_{2n}, this is an indication for the vanishing of this shell closure for these very neutron-rich nuclei. The standard behavior represented by the Ca chain seems to reappear slowly when moving to the chains of Cl and Ar. In order to determine the origin of the increase of S_{2n} for ^{44}P and ^{45}S, the present results should be compared with model calculations.

For the neutron-rich nucleus ^{42}Si, the protons confined in the $\pi d_{5/2}$ orbital ($Z = 14$ sub-shell gap) and the $N = 28$ gap together, could favor spherical configuration. Indeed, our result for the mass excess of ^{42}Si is around 3 MeV smaller than the extrapolation of the mass table [11]. This indicates that this nucleus is much more bound than what one would obtain if the Si isotopic chain would follow the standard trend of the Ca chain. This could possibly be an indication of the strong deformation of ^{42}Si.

Different theoretical approaches exist. On one hand, shell model calculations performed by Retamosa *et al.* [12], indicate that ^{42}Si has the characteristics of a doubly magic nucleus such as ^{48}Ca. More recently, the interaction has been adjusted to reproduce single-particle states in ^{35}Si [13] and the shell gap $1f_{7/2}$-$2p_{3/2}$ is steadily reduced from its initial value of 2 MeV at $Z = 20$ until almost zero at $Z = 8$. Therefore the closed-shell configuration becomes vulnerable and at some point it becomes energetically favorable to promote neutrons across the gap, recovering the cost in single-particle energies by the gain in neutron proton quadrupole correlation energy. Moreover, those calculations lead to a deformed ^{43}S ground state with spin $3/2^-$ while the spherical single-hole state $7/2^-$ would be the first-excited state, in good agreement with experimental data. On the other hand, the calculations performed by Lalazissis *et al.* [14] (relativistic Hartree Bogoliubov) predict the breaking of the $N = 28$ shell gap below ^{48}Ca with a large deformed configuration for ^{42}Si.

3.2 The N = 20 region

The value obtained for ^{23}N mass excess is considerably smaller ($\sim$ 1.5 MeV) than the extrapolation of the mass evaluation 2003 value given by Audi *et al.* [11], which is obtained assuming a regular behaviour of S_{2n}. This indicates that ^{23}N with 16 neutrons is more bound than

expected. This might be an indication for the existence of a shell closure at $N = 16$ for very neutron-rich nuclei. Also the value for the mass excess that we obtain for ^{24}O with 16 neutrons is lower than the value given in the mass table, which again indicates that ^{24}O is more bound than what was thought previously. For the Ne and the Na isotopic chains the two-neutron separation energies decrease much more steeply after $N = 16$ than after $N = 20$, which is again an indication for the existence of the shell closure $N = 16$ for this very neutron-rich nuclei. Moreover, the absence of the steep decrease after $N = 20$ for the Mg and Al chains confirms the vanishing of this spherical shell closure. Shell closure $N = 20$ starts to reappear for the less neutron-rich isotopes of the Al and Si chains. Beyond $N = 20$, for the Ne, Na and Mg isotopes, a rapid decrease of S_{2n} indicates that those isotopes may become unbound rapidly with respect to the neutron emissions. If we add one proton in the $\pi d_{5/2}$ from the oxygen configuration, the picture for the fluorine isotopes changes drastically. The S_{2n} values decrease continuously to almost zero for ^{29}F. Only strong shell effects could bind the heaviest known fluorine isotope, ^{31}F.

The shell correction energies from fig. 4 nicely show the shell effect evolution in that region and confirm the previous discussion on the experimental S_{2n} values. If we start from the O isotopes, we clearly observe two $N = 8$ and $N = 16$ minima with a rather high, 5 MeV, difference in magnitude between them (O with $N > 16$ do not exist as bound nuclei). The gap at $N = 16$ still persists when we add a proton in the $\pi d_{5/2}$ shell, but the amplitude decreases smoothly up to ^{29}Al. Moreover, the SCE confirm the vanishing of the shell closure at $N = 20$, SCE are maximized at $N = 20$ for the F, Ne, Na and Mg isotopes.

More recent shell model calculations [15] interpret this disappearance of the magic number $N = 20$ by the inversion of the order of the shells due to the dependence of the neutron-proton interaction on the combination of their spin in the nucleus (nucleon-nucleon spin-isospin V$\sigma\tau$ interaction). In that region, the basic mechanism of this change is the strongly attractive interaction between spin-orbit partners $\pi d_{5/2}$ and $\nu d_{3/2}$. As Z increases from 8 to 14, valence protons are added into the $\pi d_{5/2}$ orbit. Due to the strong attraction between a proton in $\pi d_{5/2}$ and a neutron in $\nu d_{3/2}$, as more protons are put in $\pi d_{5/2}$, a neutron in $\nu d_{3/2}$ is more strongly bound. The magic number $N = 20$ should be therefore replaced by $N = 16$ for the nuclei in this region very far from stability, and that this phenomenon should occur over all the chart of the nuclei. In particular, the non-observance of ^{28}O, a doubly magic nucleus in theory, could also be explained by this modification of its shell structure.

4 Conclusions

The direct time-of-flight method with SPEG is a powerful method for measuring masses up to the neutron drip-line in the mass region $A \sim 10$–50. This paper presents preliminary results of 8 new masses and 37 masses measured with a better precision than previously. The final result will be published in a future publication. The experimental shell corrections and the two neutron separation energies have been calculated. The results thus obtained provide a means of identifying new nuclear structure effects that are well illustrated by this work in the $N = 16$, $N = 20$ and $N = 28$ region.

ACCV acknowledges his partial support by the U.S. Department of Energy, Office of Nuclear Physics, under contract W-31-109-ENG-38. This work was particularly supported by the INTAS-00-00463, by the Russian Foundation for Fundamental Research (RFFR) and PICS (IN2P3) No. 1171.

References

1. B. Pfeiffer *et al.*, Z. Phys. A **357**, 235 (1997).
2. L. Bianchi *et al.*, Nucl. Instrum. Methods Phys. Res. A **276**, 509 (1989).
3. R. Anne, Nucl. Instrum. Methods Phys. Res. B **126**, 279 (1997).
4. F. Sarazin, Thesis GANIL T 99 03 (1999).
5. H. Savajols, Hyperfine Interact. **132**, 245 2001.
6. P. Moller, J.R. Nix, At. Data Nucl. Data Tables **59**, 185 (1995).
7. F. Sarazin *et al.*, Phys. Rev. Lett. **84**, 5062 (2000).
8. H. Scheit *et al.*, Phys. Rev. Lett. **77**, 3967 (1996).
9. T. Glasmacher *et al.*, Phys. Lett. B **395**, 163 (1997).
10. D. Sohler *et al.*, Phys. Rev. C **66**, 054302 (2002).
11. G. Audi *et al.*, Nucl. Phys. A **729**, 2003 3.
12. J. Retamosa *et al.*, Phys. Rev. C **55**, 1266 (1997).
13. S. Nummela *et al.*, Phys. Rev. C **63**, 044316 (2001).
14. G.A. Lalazissis *et al.*, Phys. Rev. C **60**, 014310 (1999).
15. T. Otsuka *et al.*, Phys. Rev. Lett. **87**, 082502 (2001).